Application of the Perfectly Matched Absorbing Layer Model to the Linear Elastodynamic Problem in Anisotropic Heterogeneous Media

Francis Collino* and **Chrysoula Tsogka**†

(February 16, 2000)

ABSTRACT

We present and analyze a perfectly matched, absorbing layer model for the velocity-stress formulation of elastodynamics. The principle idea of this method consists in introducing an absorbing layer in which we decompose each component of the unknown into two auxiliary components: a component orthogonal to the boundary and a component parallel to it. A system of equations governing these new unknowns is then constructed. A damping term is finally introduced for the component orthogonal to the boundary. This layer model has the property of generating no reflection at the interface between the free medium and the artificial absorbing medium. In practice, both the boundary condition introduced at the outer boundary of the layer and the dispersion due to the numerical scheme produce a small reflection which can be controled even with very thin layers. As we will show with several experiments, this model gives very satisfactory results, namely the reflection coefficient, even in the case of heterogeneous, anisotropic media, is about 1% (resp. 0.01%) for a layer thickness of five (resp. twenty) space discretization steps.

*INRIA-Rocquencourt, Domaine de Voluceau, B.P. 105, F-78153 Le Chesnay Cdex.
†INRIA-Rocquencourt, Domaine de Voluceau, B.P. 105, F-78153 Le Chesnay Cdex.

INTRODUCTION

The simulation of waves by finite-difference or finite-element methods in unbounded domains requires a special treatment for the boundaries of the necessarily truncated computational domain. Two solutions have been proposed for this purpose : absorbing boundary conditions (ABC's) and absorbing layers. ABC's were introduced by B. Engquist and A. Majda (1977) for the acoustic wave equation. They consist in introducing some suitable local boundary conditions that simulate the outgoing nature of the waves impinging on the borders. This method works particularly well for absorbing waves nearly normally incident to the artificial boundaries. For waves traveling obliquely to the boundary, higher order ABC must be used to achieve acceptable accuracy, (Hagstrom, 1997).

For elastic waves, the situation is more complex. First, the transparent condition, i.e. the exact condition relating normal stress and displacement on a line for outgoing waves, is no longer a scalar but a matrix integro-differential relation. Its approximation by partial differential equations, which is the usual way to construct ABC's, leads to a very complex system of equations, especially for higher order methods. The stability of the coupled problem composed of the elastodynamic system completed by these artificial conditions is then very difficult to analyze and the situation is even more intricate when discretization is considered, (Chalindar, 1987). To overcome these difficulties, Higdon (1991), (1992), proposed to combine several first order boundary conditions designed for the wave equation, each of them being associated with either the pressure wave velocity or the shear wave velocity. These conditions are theoretically stable, (Higdon, 1990), relatively easy to implement and efficient for waves traveling in a direction close to the normal of the artificial boundaries. They can be adapted to the case of surface waves too, (Sochacki et al., 1987). However, for other directions of propagation, important spurious reflections may occur. Some authors, (Peng and Toksoz, 1995) for instance, have proposed to optimize the coefficients of Higdon's method in order to make these reflections decrease. However, numerical experiments still show relatively strong spurious reflections in some situations and stability problems when higher order numerical schemes are used, (Simone and Hestholm, 1998).

Layer models are an alternative to ABC's. The idea is to surround the domain of interest by some artificial absorbing layers in which waves are trapped and attenuated. For elastic waves, several models have been proposed. For instance, Sochacki et al., (1987) suggest adding inside the layers some attenuation term, proportional to the first time derivative of the displacement to the elastodynamic equations. This technique, inspired by physics, is quite delicate in practice. The main difficulty is that, when entering the layers, the wave "sees" the change in impedance of the medium and then is reflected artificially into the domain of interest. The use of smooth and not too high attenuation profiles allows us to weaken the difficulty but requires the use of thick layers, (Israeli and Orszag, 1981).

In this paper, we propose to adapt a layer technique introduced in (Bérenger, 1994) for Maxwell's equations by Bérenger and that is now the most widely used method for the simulation of electromagnetic waves in non bounded domains, (Bérenger, 1996), (1997), (Zhao and Cangellaris, 1996), (Teixeira and Chew, 1998), (Turkel and Yefet, 1998). This technique consists in designing an absorbing layer called a perfectly matched layer (PML) that possesses the property of generating no reflection at the interface between the free medium and the artificial absorbing medium. This property allows us to use a very high damping parameter inside the layer and consequently a small layer width while achieving a quasi-perfect absorption of the waves. To our knowledge, this method has already been used only once for elastic waves simulation. In (Hastings et al., 1996), the authors propose the use of PML for the compressional and shear potentials formulation. In our paper, the PML are incorporated in the stress-velocity formulation.

The present paper is organized as follows. In section II we construct the PML model in the general case of an evolution problem. It is based on an interpretation of the PML model of Brenger (1994) as a change of variable in the complex plane c.f (Rappaport, 1995), (Collino, 1996). In section III, we apply the previous model to the velocity stress formulation for elastodynamics and we study the properties of the continuous PML model via a plane wave analysis. In order to show the generality of the PML model, two numerical schemes are presented (section IV). The first one is the classical Virieux finite-differences scheme (Virieux, 1986) while the second one is a mixed finite-element scheme (Bécache et al., 1997) which allows us to consider anisotropic media as well. Finally in section V we present several numerical results which show the efficiency of this model even in the case of heterogeneous, anisotropic elastic media and its superiority when compared to the classical ABC method.

PML MODEL FOR A GENERAL EVOLUTION PROBLEM

We will present in this section the basic principles of the PML model in the general case of an evolution problem. This will allow us to generalize it to other models of wave propagation. Consider a general evolution problem of the following form

$$\begin{aligned} &(a)\ \ \partial_t v - A\partial_x v - B\partial_y v = 0\ , \\ &(b)\ \ v(t=0) = v_0\ . \end{aligned} \tag{1}$$

where in the general case v is a m-vector, A is a $m \times m$ matrix, $x \in \mathbb{R}$ and $y \in \mathbb{R}^{n-1}$. To simplify the presentation, in what follows we consider the scalar case with

$m = 1$ and $n = 2$. Moreover, we assume that the initial condition v_0 is zero on the right half space. We would like to replace problem (1) by an equivalent one posed in the left half-space. The basic principle of the PML model, is *to couple the equation in the left half-space with an equation in the right half-space such that there is* **no reflection** *at the interface, and that the wave* **decreases exponentially** *inside the right half space.* Thus, we first introduce the following system

$$\begin{aligned} &\partial_t v^{\|} - B\partial_y v = 0 \ , \\ &\partial_t v^{\perp} - A\partial_x v = 0 \ , \end{aligned} \tag{2}$$

with $v = v^{\|} + v^{\perp}$, and where superscript $\|$ means that we keep only the derivative parallel to the interface, i.e. the y-derivative (while superscript $\perp$ means that only the x-derivative is considered). It is easy to see that system (2) implies (1)-(a). Secondly, we introduce a function $d(x)$, zero on the left half space and positive on the right half space. This function will play the role of the damping factor. We define now a new wave, u, solution of the following system

$$\begin{aligned} &\partial_t u^{\perp} + d(x)u^{\perp} - A\partial_x u = 0 \ , \\ &\partial_t u^{\|} - B\partial_y u = 0 \ , \\ &u(t=0) = v_0 \ , \end{aligned} \tag{3}$$

with $u = u^{\|} + u^{\perp}$. It is easy to see that u satisfies the same system of equations as v in the left half space. If we look for time harmonic solutions of system (1) with angular frequency ω, we get

$$i\omega\hat{v} - A\partial_x\hat{v} - B\partial_y\hat{v} = 0 \ .$$

In the same way, the time harmonic solutions of system (3) satisfy

$$\begin{aligned} &(i\omega + d(x))\hat{u}^{\perp} - A\partial_x\hat{u} = 0 \ , \\ &i\omega\hat{u}^{\|} - B\partial_y\hat{u} = 0 \ , \end{aligned}$$

with $\hat{u} = \hat{u}^{\|} + \hat{u}^{\perp}$, or, equivalently,

$$\begin{aligned} &i\omega\hat{u}^{\perp} - \frac{i\omega}{i\omega + d(x)}A\partial_x\hat{u} = 0 \ , \\ &i\omega\hat{u}^{\|} - B\partial_y\hat{u} = 0 \ , \end{aligned}$$

with $\hat{u} = \hat{u}^{\|} + \hat{u}^{\perp}$. We can remark now, that the PML model consists in the simple substitution

$$\partial_x \to \partial_{\tilde{x}} = \frac{i\omega}{i\omega + d(x)}\partial_x \ ,$$

which implies the complex change of variables

$$\tilde{x}(x) = x - \frac{i}{\omega}\int_0^x d(s)ds \ .$$

We can study now the properties of this model using a plane wave analysis. We seek particular solutions of system (1) in the following form

$$\begin{aligned} &v = v_0\exp[-i(k_x x + k_y y - \omega t)], \\ &k = (k_x, k_y) \in \mathbb{R}\times\mathbb{R}, \ \omega \in \mathbb{R} \ . \end{aligned} \tag{4}$$

Formula (4) is a plane wave propagating in the direction k with the phase velocity $\omega/|k|$. In order to be a solution of problem (1), v has to satisfy the following relation

$$iv_0\omega - iAv_0k_x - iBv_0k_y = 0 \ . \tag{5}$$

In the same way, we seek particular solutions of system (3) in the following form

$$\begin{aligned} &u^{\|} = a^{\|}\exp[-i(k_x\tilde{x}(x) + k_y y - \omega t)] \ , \\ &u^{\perp} = a^{\perp}\exp[-i(k_x\tilde{x}(x) + k_y y - \omega t)] \ , \\ &u = u^{\|} + u^{\perp} \ . \end{aligned}$$

In order to be a solution of problem (3), $u^{\|}$ and $u^{\perp}$ have to satisfy the following relations

$$\begin{aligned} &ia^{\|}\omega - iB(a^{\perp} + a^{\|})k_y = 0 \ , \\ &(i\omega + d(x))a^{\perp} - i\left(1 - \frac{id(x)}{\omega}\right)A(a^{\perp} + a^{\|})k_x = 0 \ , \end{aligned} \tag{6}$$

or, equivalently

$$\begin{aligned} &ia^{\|}\omega - iB(a^{\perp} + a^{\|})k_y = 0 \ , \\ &ia^{\perp}\omega - iA(a^{\perp} + a^{\|})k_x = 0 \ . \end{aligned} \tag{7}$$

Adding the two equalities of (7), gives

$$i(a^{\perp} + a^{\|})\omega - iA(a^{\perp} + a^{\|})k_x - iB(a^{\perp} + a^{\|})k_y = 0 \ . \tag{8}$$

We can remark now that if we chose $a^{\perp}$ and $a^{\|}$ such that

$$a^{\perp} + a^{\|} = v_0,$$

equation (8) becomes the same as (5). Moreover from (7) we get

$$a^{\|} = Bv_0\frac{k_y}{\omega}, \qquad a^{\perp} = Av_0\frac{k_x}{\omega} \ , \tag{9}$$

which gives the plane wave solution of (3). We then have the following property:
The plane wave solution of system (3) can be written in the form

$$u \ = v_0 \ \exp[-i(k_x x + k_y y - \omega t)] \ \exp[-\frac{k_x}{\omega}\int_0^x d(s)ds] \ ,$$

and satisfies :

- *$u \equiv v$ in the left half-space, $x \leq 0$, which means that we have no reflection at the interface : the layer model is perfectly matched.*
- *u is damped in the right half-space,*

- *the damping coefficient in the absorbing half space is*

$$\alpha_d = \frac{\|u(x)\|}{\|v(x)\|} = \exp[-\frac{k_x}{\omega}\int_0^x d(s)ds] \ . \qquad (10)$$

Remark 1 *Relation (10) implies that the waves decrease exponentially in the absorbing half space. The damping coefficient (α_d) depends on the direction of propagation of the wave. More precisely, α_d, decreases very fast for a wave propagating normally to the interface and decreases more and more slowly as the direction of propagation approaches the parallel to the interface.*

PML MODEL FOR ELASTODYNAMICS

In this section we present the PML model for the continuous elastodynamic problem. As we have seen in section II, we know how to construct a PML model for an evolution problem of the form (1). Thus, in order to apply the technique described in the previous section to elastodynamics, we need to write the elastodynamic problem in the form of system (1). This can be easily done once we consider the mixed velocity-stress formulation for elastodynamics.

The elastodynamic problem

We consider the 2D elastodynamic problem written as a first order hyperbolic system, the so called velocity-stress system

$$\begin{aligned} \varrho\partial_t v - \mathbf{div}\sigma &= 0 \ , \\ A\partial_t\sigma - \varepsilon(v) &= 0 \ , \end{aligned} \qquad (11)$$

together with initial conditions. We suppose, as in the previous section, that the initial condition is supported in the left half space. In (11) $v = (v_x, v_y)$ denotes the velocity, σ the stress tensor and $\varrho = \varrho(x)$ the density. If $u = (u_x, u_y)$ is the displacement, then $v = \partial_t u$. We denote $\varepsilon(u)$ the linearized strain tensor, i.e.,

$$\varepsilon_{ij}(u) = \frac{1}{2}\left(\partial_j u_i + \partial_i u_j\right) \ .$$

The stress tensor is related to the strain tensor by the generalized Hooke's law

$$\sigma = \sigma(u)(x,t) = C(x)\varepsilon(u)(x,t) \ ,$$

where stiffness $C(x)$ is a 4×4 positive tensor having the classical properties of symmetry (Auld, 1973). In system (11) we used the compliance tensor

$$A = A(x) = C^{-1}(x) \ .$$

Finally, we identify the stress tensor σ with the following vector (still denoted by σ)

$$\begin{aligned} &\sigma = [\sigma_1,\ \sigma_2,\ \sigma_3]^T \ , \\ &\sigma_1 = \sigma_{xx} \ ; \ \sigma_2 = \sigma_{yy} \ ; \ \sigma_3 = \sigma_{xy} \ . \end{aligned}$$

We can write (11) in the following matrix form

$$\begin{aligned} \varrho\partial_t v &= D^{\|}\partial_y\sigma + D^{\perp}\partial_x\sigma \ \text{ in } \Omega \ , \\ A\partial_t\sigma &= E^{\|}\partial_y v + E^{\perp}\partial_x v \ \text{ in } \Omega \ , \end{aligned}$$

with

$$D^{\|} = \begin{bmatrix} 0 & 0 & 1 \\ 0 & 1 & 0 \end{bmatrix}, \quad D^{\perp} = \begin{bmatrix} 1 & 0 & 0 \\ 0 & 0 & 1 \end{bmatrix},$$

$$E^{\|} = \begin{bmatrix} 0 & 0 & 1 \\ 0 & 1 & 0 \end{bmatrix}^T, \quad E^{\perp} = \begin{bmatrix} 1 & 0 & 0 \\ 0 & 0 & 1 \end{bmatrix}^T \ .$$

We can apply now the same technique as in section II and we get the following system in the Perfectly Matched Layer($x > 0$)

$$\begin{aligned} &v = v^{\|} + v^{\perp} && ; \ \sigma = \sigma^{\|} + \sigma^{\perp} \ , \\ &\varrho\partial_t v^{\|} = D^{\|}\partial_y\sigma && ; \ A\partial_t\sigma^{\|} = E^{\|}\partial_y v \ , \\ &\varrho\partial_t v^{\perp} + d(x)v^{\perp} = D^{\perp}\partial_x\sigma && ; \ A\sigma^{\perp} = E^{\perp}\partial_x v \ , \end{aligned}$$

where $d(x)$ denotes the damping factor. In an homogeneous, isotropic elastic medium, the matrix $C(x)$ depends on the Lam coefficients $(\lambda,\ \mu)$ of the medium. In this case the PML model can be written in the following form

$$\begin{aligned} &v = v^{\|} + v^{\perp} && ; \ \sigma = \sigma^{\|} + \sigma^{\perp}, \\ &\varrho\,(\partial_t + d(x))v_x^{\perp} = \partial_x\sigma_{xx} && ; \ \varrho\,\partial_t v_x^{\|} = \partial_y\sigma_{xy}, \\ &\varrho\,(\partial_t + d(x))v_y^{\perp} = \partial_x\sigma_{xy} && ; \ \varrho\,\partial_t v_y^{\|} = \partial_y\sigma_{yy}, \\ &(\partial_t + d(x))\sigma_{xx}^{\perp} = (\lambda+2\mu)\partial_x v_x && ; \ \partial_t\sigma_{xx}^{\|} = \lambda\partial_y v_y, \\ &(\partial_t + d(x))\sigma_{yy}^{\perp} = \lambda\partial_x v_x && ; \ \partial_t\sigma_{yy}^{\|} = (\lambda+2\mu)\partial_y v_y, \\ &(\partial_t + d(x))\sigma_{xy}^{\perp} = \mu\partial_x v_y && ; \ \partial_t\sigma_{xy}^{\|} = \mu\partial_y v_x. \end{aligned} \qquad (12)$$

Plane wave analysis

Infinite absorbing layer.—In the case of a homogeneous, isotropic elastic medium, following the same technique as in section II, we can show that the displacement plane waves, $U_j,\ j = p,\ s$, corresponding to solutions of system (11) can be written in the following form

$$\begin{aligned} U_p &= A_p\vec{d}_p\exp[i\omega V_p(t - \frac{\cos(\theta)x + \sin(\theta)y}{V_p})] \ , \\ U_s &= A_s\vec{d}_s\exp[i\omega V_s(t - \frac{-\sin(\theta)x + \cos(\theta)y}{V_s})] \ , \end{aligned} \qquad (13)$$

where $V_p = \sqrt{(\lambda + 2\mu)/\varrho}$ is the pressure wave velocity, $V_s = \sqrt{\mu/\varrho}$ is the shear wave velocity, θ gives the direction of wave propagation, $\vec{d}_j,\ j = p,\ s$, defines the direction of particle motion and $A_j,\ j = p,\ s$ is the amplitude of the wave. We can remark then that the displacement plane waves, $\widetilde{U}_j$ (for $j = p,\ s$), solutions of system (12) can be written as

$$
\begin{aligned}
\widetilde{U}_p &= A_p \vec{d}_p \exp[i\omega V_p (t - \frac{\cos(\theta)\tilde{x}_p + \sin(\theta) y}{V_p})] \ , \\
\widetilde{U}_s &= A_s \vec{d}_s \exp[i\omega V_s (t - \frac{-\sin(\theta)\tilde{x}_s + \cos(\theta) y}{V_s})] \ ,
\end{aligned}
\qquad (14)
$$

where we simply substituted $\tilde{x}_j,\ j = p,\ s$ for x in (13), with $\tilde{x}_j,\ j = p,\ s$, defined in the same way as in section II (ω replaced by ωV_j)

$$
\tilde{x}_j(x) = x - \frac{i}{\omega V_j} \int_0^x d(s) ds, \quad j = p,\ s \ .
$$

Moreover it can be shown that $\widetilde{U}_j, j = p, s$, satisfies :

- $\widetilde{U}_j \equiv U_j$, for $j = p,\ s$, in the left half-space $x \leq 0$ (no reflection),
- $\widetilde{U}_j$, $j = p,\ s$, is damped in the right half-space,
- the damping coefficient in the absorbing layer is

$$
\begin{aligned}
\frac{\|\widetilde{U}_p(x)\|}{\|U_p(x)\|} &= \exp[-\frac{\cos\theta}{V_p} \int_0^x d(s) ds], \\
\frac{\|\widetilde{U}_s(x)\|}{\|U_s(x)\|} &= \exp[-\frac{\cos\theta}{V_s} \int_0^x d(s) ds] \ .
\end{aligned}
$$

Finite absorbing layer.—In practice, we take a finite absorbing layer by introducing a boundary at $x = \delta$, with a Dirichlet condition. This new boundary produces a reflection, but since the wave decreases exponentially in the layer, the reflection coefficient becomes quickly very small. This coefficient depends on the choice of $d(x)$ and on the size δ of the layer. In order to study the properties of the model in this case, we recall some classical results for the elastodynamic problem.

Consider the elastodynamic problem with a homogeneous Dirichlet condition($\vec{v} = 0$) on the boundary $x = 0$ as shown in Figure 1. Take for example the case of an incident plane wave P

$$
U_p^{inc} = A_{inc} \vec{d}_p \exp[i\omega V_p (t - \frac{\vec{d}_p \cdot \vec{x}}{V_p})], \ \vec{d}_p = (\cos\theta, \sin\theta).
$$

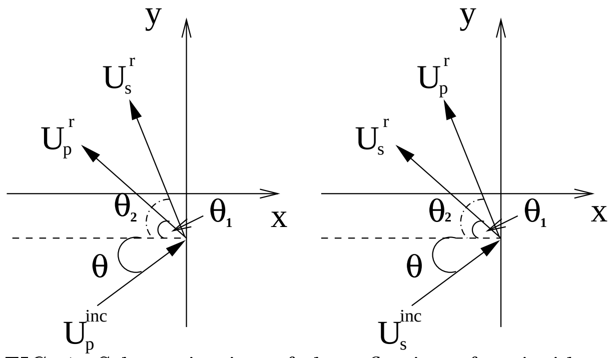

FIG. 1. Schematic view of the reflection of an incident P wave (left) and of an incident S wave (right) in the case of a homogeneous Dirichlet boundary condition.

We know then (cf. (Achenbach, 1984), vol 1, §5.6, p. 173) that the incident wave is reflected into a pressure wave U_p^r and a shear wave U_s^r given by

$$
\begin{aligned}
U_p^r &= A_p^r \vec{d}_p^r \exp[i\omega V_p (t - \frac{\vec{d}_p^r \cdot \vec{x}}{V_p})], \quad \vec{d}_p^r = (-\cos\theta_1, \sin\theta_1) \ , \\
U_s^r &= A_s^r \vec{d}_s^r \exp[i\omega V_p (t - \frac{\vec{p}_s \cdot \vec{x}}{V_p})], \quad \vec{d}_s^r = (-\sin\theta_2, \cos\theta_2), \\
& \qquad \vec{p}_s = (\cos\theta_2, \sin\theta_2) \ ,
\end{aligned}
$$

and we have the reflection coefficients

$$
\begin{aligned}
R_{pp} &= \frac{\|U_p^r\|}{\|U_p^{inc}\|} = \frac{\cos(\theta - \theta_2)}{\cos(\theta + \theta_2)}, \\
R_{ps} &= \frac{\|U_s^r\|}{\|U_p^{inc}\|} = \frac{\sin\theta_2}{\cos(\theta + \theta_2)},
\end{aligned}
$$

with $\sin\theta_2 = V_s \ \sin\theta / V_p$. In the same way in the case of an incident plane wave S we have

$$
\begin{aligned}
R_{ss} &= \frac{\|U_s^r\|}{\|U_s^{inc}\|} = \frac{\sin(\theta + \theta_2)}{\sin(\theta - \theta_2)} \ , \\
R_{sp} &= \frac{\|U_p^r\|}{\|U_s^{inc}\|} = \frac{\sin\theta_2}{\sin(\theta - \theta_2)} \ ,
\end{aligned}
$$

with $\cos\theta_2 = V_p \ \cos\theta / V_s$. We can consider now the case of the finite layer. Given that the plane waves, $U_j,\ j = p,\ s$, corresponding to solutions of system (11) are given by equations (13), we can compute the reflection coefficients induced by the layer of width δ.

The case of a plane wave P

As we have shown previously there is no reflection at the interface $x = 0$ when the plane wave $\widetilde{U}_p$ penetrates the lossy medium. After traveling a length δ we can compute $\widetilde{U}_p$ using the formula (14), obtaining

$$
\widetilde{U}_p = U_p \exp[-\frac{\cos\theta}{V_p} \int_0^\delta d(s) ds] \ .
$$

Then the plane wave $\widetilde{U}_p$, gives at the boundary $x = \delta$, two reflected waves $\widetilde{U}_p^r$ and $\widetilde{U}_s^r$, which are damped till penetrating again the elastic medium at the interface $x =$

0. It is easy to see that the reflection coefficient is given in this case by

$$R^\delta_{pp} = \frac{\|\widetilde{U}^r_p(x)\|}{\|U_p(x)\|} = R_{pp}\exp[-2\frac{\cos\theta}{V_p}\int_0^\delta d(s)ds],\ x<0\ ,$$
$$R^\delta_{ps} = \frac{\|\widetilde{U}^r_s(x)\|}{\|U_p(x)\|} = R_{ps}\exp[-2\frac{\cos\theta}{V_p}\int_0^\delta d(s)ds],\ x<0\ . \tag{15}$$

The case of a plane wave S

In the case of an incident plane wave S, we obtain similarly

$$R^\delta_{ss} = \frac{\|\widetilde{U}^r_s(x)\|}{\|U_s(x)\|} = R_{ss}\exp[-2\frac{\cos\theta}{V_s}\int_0^\delta d(s)ds],\ x<0\ ,$$
$$R^\delta_{sp} = \frac{\|\widetilde{U}^r_p(x)\|}{\|U_s(x)\|} = R_{sp}\exp[-2\frac{\cos\theta}{V_s}\int_0^\delta d(s)ds],\ x<0\ . \tag{16}$$

Remark 2 *Relations (15) and (16) imply that the reflection can be made as weak as desired by choosing the damping factor $d(x)$ large enough. However this is no longer true when we consider the discrete PML model. As we will see in Appendix A, the discrete absorbing layer model is not perfectly matched. That is a consequence of the numerical dispersion, which introduces a reflection at the interface.*

THE DISCRETE PML MODEL

In this section we present the discrete PML model for elastodynamics. To do so we introduce two numerical schemes for the discretization of system (11). The first one is a finite-difference scheme, introduced by Virieux in (Virieux, 1986) and the second one is obtained using a new mixed finite element (Bécache et al., 1997) in a regular mesh. The use of this finite element has the advantage of leading to an explicit scheme (mass lumping), even in the case of an anisotropic elastic medium.

The Virieux finite-difference scheme

This scheme uses a staggered grid formulation, so that, if v_x is computed at the points (i,j) $(x_i = ih, y_j = jh)$ of a reference grid, then v_y is computed at the points $(i+\frac{1}{2}, j+\frac{1}{2})$, σ_{xx} and σ_{yy} at $(i+\frac{1}{2}, j)$ and σ_{xy} at $(i, j+\frac{1}{2})$. The discrete PML model associated to the Virieux finite-difference scheme can be written as follows

$$(v_x)^n_{i,j} = (v^x_x)^n_{i,j} + (v^y_x)^n_{i,j}\ ,$$
$$\frac{(v^x_x)^{n+1}_{i,j} - (v^x_x)^n_{i,j}}{\Delta t} + d^x_i\frac{(v^x_x)^{n+1}_{i,j} + (v^x_x)^n_{i,j}}{2} = \frac{(\sigma_{xx})^{n+\frac{1}{2}}_{i\frac{1}{2},j} - (\sigma_{xx})^{n+\frac{1}{2}}_{i-\frac{1}{2},j}}{\varrho h}\ ,$$
$$\frac{(v^y_x)^{n+1}_{i,j} - (v^y_x)^n_{i,j}}{\Delta t} + d^y_j\frac{(v^y_x)^{n+1}_{i,j} + (v^y_x)^n_{i,j}}{2} = \frac{(\sigma_{xy})^{n+\frac{1}{2}}_{i,j\frac{1}{2}} - (\sigma_{xy})^{n+\frac{1}{2}}_{i,j-\frac{1}{2}}}{\varrho h}\ ,$$

$$(v_y)^n_{i\frac{1}{2},j\frac{1}{2}} = (v^x_y)^n_{i\frac{1}{2},j\frac{1}{2}} + (v^y_y)^n_{i\frac{1}{2},j\frac{1}{2}}\ ,$$
$$\frac{(v^x_y)^{n+1}_{i\frac{1}{2},j\frac{1}{2}} - (v^x_y)^n_{i\frac{1}{2},j\frac{1}{2}}}{\Delta t} + d^x_{i\frac{1}{2}}\frac{(v^x_y)^{n+1}_{i\frac{1}{2},j\frac{1}{2}} + (v^x_y)^n_{i\frac{1}{2},j\frac{1}{2}}}{2} = \frac{(\sigma_{xy})^{n+\frac{1}{2}}_{i^1,j\frac{1}{2}} - (\sigma_{xy})^{n+\frac{1}{2}}_{i,j\frac{1}{2}}}{\varrho h}\ ,$$
$$\frac{(v^y_y)^{n+1}_{i\frac{1}{2},j\frac{1}{2}} - (v^y_y)^n_{i\frac{1}{2},j\frac{1}{2}}}{\Delta t} + d^y_{j\frac{1}{2}}\frac{(v^y_y)^{n+1}_{i\frac{1}{2},j\frac{1}{2}} + (v^y_y)^n_{i\frac{1}{2},j\frac{1}{2}}}{2} = \frac{(\sigma_{yy})^{n+\frac{1}{2}}_{i\frac{1}{2},j^1} - (\sigma_{xy})^{n+\frac{1}{2}}_{i\frac{1}{2},j}}{\varrho h}\ ,$$

$$(\sigma_{xx})^{n+\frac{1}{2}}_{i\frac{1}{2},j} = (\sigma^x_{xx})^{n+\frac{1}{2}}_{i\frac{1}{2},j} + (\sigma^y_{xx})^{n+\frac{1}{2}}_{i\frac{1}{2},j}\ ,$$
$$\frac{(\sigma^x_{xx})^{n+\frac{1}{2}}_{i\frac{1}{2},j} - (\sigma^x_{xx})^{n-\frac{1}{2}}_{i\frac{1}{2},j}}{\Delta t} + d^x_{i\frac{1}{2}}\frac{(\sigma^x_{xx})^{n+\frac{1}{2}}_{i\frac{1}{2},j} + (\sigma^x_{xx})^{n-\frac{1}{2}}_{i\frac{1}{2},j}}{2} = (\lambda+2\mu)\frac{(v_x)^n_{i^1,j} - (v_x)^n_{i,j}}{h}\ ,$$
$$\frac{(\sigma^y_{xx})^{n+\frac{1}{2}}_{i\frac{1}{2},j} - (\sigma^y_{xx})^{n-\frac{1}{2}}_{i\frac{1}{2},j}}{\Delta t} + d^y_j\frac{(\sigma^y_{xx})^{n+\frac{1}{2}}_{i\frac{1}{2},j} + (\sigma^y_{xx})^{n-\frac{1}{2}}_{i\frac{1}{2},j}}{2} = \lambda\frac{(v_y)^n_{i\frac{1}{2},j\frac{1}{2}} - (v_y)^n_{i\frac{1}{2},j-\frac{1}{2}}}{h}\ ,$$

$$(\sigma_{yy})^{n+\frac{1}{2}}_{i\frac{1}{2},j} = (\sigma^x_{yy})^{n+\frac{1}{2}}_{i\frac{1}{2},j} + (\sigma^y_{yy})^{n+\frac{1}{2}}_{i\frac{1}{2},j}\ ,$$
$$\frac{(\sigma^x_{yy})^{n+\frac{1}{2}}_{i\frac{1}{2},j} - (\sigma^x_{yy})^{n-\frac{1}{2}}_{i\frac{1}{2},j}}{\Delta t} + d^x_{i\frac{1}{2}}\frac{(\sigma^x_{yy})^{n+\frac{1}{2}}_{i\frac{1}{2},j} + (\sigma^x_{yy})^{n-\frac{1}{2}}_{i\frac{1}{2},j}}{2} = \lambda\frac{(v_x)^n_{i^1,j} - (v_x)^n_{i,j}}{h}\ ,$$
$$\frac{(\sigma^y_{yy})^{n+\frac{1}{2}}_{i\frac{1}{2},j} - (\sigma^y_{yy})^{n-\frac{1}{2}}_{i\frac{1}{2},j}}{\Delta t} + d^y_j\frac{(\sigma^y_{yy})^{n+\frac{1}{2}}_{i\frac{1}{2},j} + (\sigma^y_{yy})^{n-\frac{1}{2}}_{i\frac{1}{2},j}}{2} = (\lambda+2\mu)\frac{(v_y)^n_{i\frac{1}{2},j\frac{1}{2}} - (v_y)^n_{i\frac{1}{2},j-\frac{1}{2}}}{h}\ ,$$

$$(\sigma_{xy})^{n+\frac12}_{i,j^{\frac12}} = (\sigma^x_{xy})^{n+\frac12}_{i,j^{\frac12}} + (\sigma^y_{xy})^{n+\frac12}_{i,j^{\frac12}} ,$$

$$\frac{(\sigma^x_{xy})^{n+\frac12}_{i,j^{\frac12}} - (\sigma^x_{xy})^{n-\frac12}_{i,j^{\frac12}}}{\Delta t} + d^x_i \frac{(\sigma^x_{xy})^{n+\frac12}_{i,j^{\frac12}} + (\sigma^x_{xy})^{n-\frac12}_{i,j^{\frac12}}}{2} = \mu \frac{(v_y)^n_{i^{\frac12},j^{\frac12}} - (v_y)^n_{i^{-\frac12},j^{\frac12}}}{h} ,$$

$$\frac{(\sigma^y_{xy})^{n+\frac12}_{i,j^{\frac12}} - (\sigma^y_{xy})^{n-\frac12}_{i,j^{\frac12}}}{\Delta t} + d^y_{j^{\frac12}} \frac{(\sigma^y_{xy})^{n+\frac12}_{i,j^{\frac12}} + (\sigma^y_{xy})^{n-\frac12}_{i,j^{\frac12}}}{2} = \mu \frac{(v_x)^n_{i,j^1} - (v_x)^n_{i,j}}{h} .$$

where we used the notation $i^k = i + k$ and $j^k = j + k$. The previous system of equations corresponds to the PML model in the corners, where we need damping in both directions. For the computation of the solution inside the PML layers in the x direction we use the same system of equations with $d^y = 0$, while for PML layers in the y direction we take $d^x = 0$. We present in Figure 2 the values of d^x and d^y for the different PML layers.

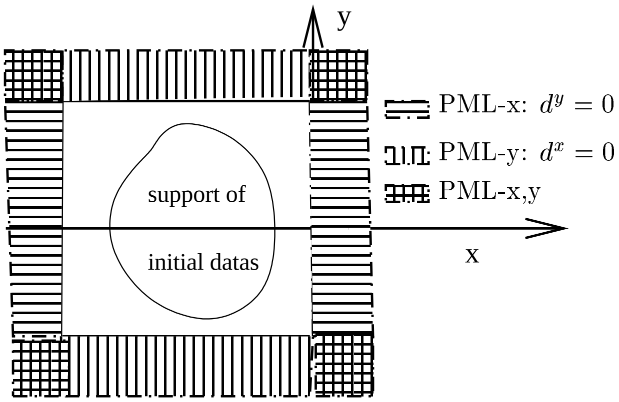

FIG. 2. The different PML layers : in the corners both d^x and d^y are positive while $d^y = 0$ (resp. $d^x = 0$) inside the PML layers in the x (resp. y) direction.

The finite-element scheme

For this scheme, the velocity is approximated by piecewise constant functions and the stress tensor σ by piecewise linear functions with some particular continuity properties. More precisely, σ_{xy} is continuous in both directions and σ_{xx} (resp. σ_{yy}) is continuous only in the x (resp. y) direction. We present in Figure 3 the mixed finite element used.

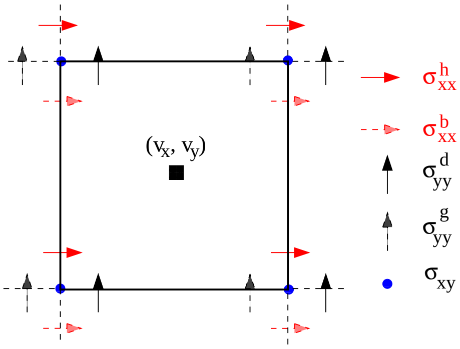

FIG. 3. The finite element : for the stress tensor five degrees of freedom are associated at each summit of the element and for the velocity two degrees of freedom are associated at the center of the element.

On a regular grid, the velocity $v = (v_x, v_y)$ is computed at the points $(i^{\frac12}, j^{\frac12})$ and the stress tensor at the points (i, j). We consider the general case of an anisotropic elastic material described by the elasticity matrix C, and we denote by A the inverse of C

$$A = C^{-1} = \begin{bmatrix} a_{11} & a_{12} & a_{13} \\ a_{12} & a_{22} & a_{23} \\ a_{13} & a_{23} & a_{33} \end{bmatrix} .$$

The numerical scheme can then be written in the following way (see (Bécache et al., 1998) for details). For the first equation of system (11) we have

$$\frac{(v_x)^{n+1}_{i^{\frac12},j^{\frac12}} - (v_x)^n_{i^{\frac12},j^{\frac12}}}{\Delta t} = \frac{1}{2\varrho h} \Big((\sigma^h_{xx})^{n+\frac12}_{i^1,j} - (\sigma^h_{xx})^{n+\frac12}_{i,j} + (\sigma^b_{xx})^{n+\frac12}_{i^1,j^1} - (\sigma^b_{xx})^{n+\frac12}_{i,j^1} + (\sigma_{xy})^{n+\frac12}_{i,j^1} - (\sigma_{xy})^{n+\frac12}_{i,j} + (\sigma_{xy})^{n+\frac12}_{i^1,j^1} - (\sigma_{xy})^{n+\frac12}_{i^1,j} \Big) ,$$

$$\frac{(v_y)^{n+1}_{i^{\frac12},j^{\frac12}} - (v_y)^n_{i^{\frac12},j^{\frac12}}}{\Delta t} = \frac{1}{2\varrho h} \Big((\sigma_{xy})^{n+\frac12}_{i^1,j} - (\sigma_{xy})^{n+\frac12}_{i,j} + (\sigma_{xy})^{n+\frac12}_{i^1,j^1} - (\sigma_{xy})^{n+\frac12}_{i,j^1} + (\sigma^d_{yy})^{n+\frac12}_{i,j^1} - (\sigma^d_{yy})^{n+\frac12}_{i,j} + (\sigma^g_{yy})^{n+\frac12}_{i^1,j^1} - (\sigma^g_{yy})^{n+\frac12}_{i^1,j} \Big) .$$

The second equation of system (11) results in the following 5×5 local system, coupling the five degrees of freedom associated to σ at each vertex (see Figure 3).

$$\frac{\Sigma^{n+\frac12}_{i,j} - \Sigma^{n-\frac12}_{i,j}}{\Delta t} = A_h^{-1} B_h^x + A_h^{-1} B_h^y ,$$

where

$$\Sigma = \left[\sigma^h_{xx},\ \sigma^b_{xx},\ \sigma^d_{yy},\ \sigma^g_{yy}, \sigma_{xy}\right]^t ,$$

$$
A_h = \frac{1}{2}\begin{bmatrix} 2a_{11} & 0 & a_{12} & a_{12} & 2a_{13} \\ 0 & 2a_{11} & a_{12} & a_{12} & 2a_{13} \\ a_{12} & a_{12} & 2a_{22} & 0 & 2a_{23} \\ a_{12} & a_{12} & 0 & 2a_{22} & 2a_{23} \\ 2a_{13} & 2a_{13} & 2a_{23} & 2a_{23} & 4a_{33} \end{bmatrix} ,
$$

and

$$
\begin{aligned}
B_h^x &= \frac{1}{h}\,[B_1^x,\ B_2^x,\ 0,\ 0,\ B_5^x]^t \ , \\
B_h^y &= \frac{1}{h}\,[0,\ 0,\ B_3^y,\ B_4^y,\ B_5^y]^t \ ,
\end{aligned}
$$

with

$$
\begin{aligned}
B_1^x &= (v_x)^n_{i\frac{1}{2},j\frac{1}{2}} - (v_x)^n_{i-\frac{1}{2},j\frac{1}{2}} \ , \\
B_2^x &= (v_x)^n_{i\frac{1}{2},j-\frac{1}{2}} - (v_x)^n_{i-\frac{1}{2},j-\frac{1}{2}} \ , \\
B_3^y &= (v_y)^n_{i\frac{1}{2},j\frac{1}{2}} - (v_y)^n_{i\frac{1}{2},j-\frac{1}{2}} \ , \\
B_4^y &= (v_y)^n_{i-\frac{1}{2},j\frac{1}{2}} - (v_y)^n_{i-\frac{1}{2},j-\frac{1}{2}} \ , \\
B_5^x &= (v_y)^n_{i\frac{1}{2},j\frac{1}{2}} - (v_y)^n_{i-\frac{1}{2},j\frac{1}{2}} + (v_y)^n_{i\frac{1}{2},j-\frac{1}{2}} - (v_y)^n_{i-\frac{1}{2},j-\frac{1}{2}} \ , \\
B_5^y &= (v_x)^n_{i\frac{1}{2},j\frac{1}{2}} - (v_x)^n_{i\frac{1}{2},j-\frac{1}{2}} + (v_x)^n_{i-\frac{1}{2},j\frac{1}{2}} - (v_x)^n_{i-\frac{1}{2},j-\frac{1}{2}} \ .
\end{aligned}
$$

In the case of an isotropic elastic material the matrix A_h^{-1} is given by

$$
A_h^{-1} = \begin{bmatrix} a & c & b & b & 0 \\ c & a & b & b & 0 \\ b & b & a & c & 0 \\ b & b & c & a & 0 \\ 0 & 0 & 0 & 0 & d \end{bmatrix} ,
$$

with

$$
a = \frac{2(\lambda+2\mu)^2-\lambda^2}{2(\lambda+2\mu)},\quad b = \frac{\lambda}{2},\quad c = \frac{\lambda^2}{2(\lambda+2\mu)},\quad d = \frac{\mu}{2} \ . \tag{17}
$$

We can write now the PML model associated to this scheme, using the same technique as for the Virieux scheme

$$
\begin{aligned}
&(v_x)^n_{i\frac{1}{2},j\frac{1}{2}} = (v_x^x)^n_{i\frac{1}{2},j\frac{1}{2}} + (v_x^y)^n_{i\frac{1}{2},j\frac{1}{2}} \ , \\
&\frac{(v_x^x)^{n+1}_{i\frac{1}{2},j\frac{1}{2}} - (v_x^x)^n_{i\frac{1}{2},j\frac{1}{2}}}{\Delta t} + d^x_{i\frac{1}{2}}\frac{(v_x^x)^{n+1}_{i\frac{1}{2},j\frac{1}{2}} + (v_x^x)^n_{i\frac{1}{2},j\frac{1}{2}}}{2} \\
&= \frac{1}{2\varrho h}\left((\sigma^h_{xx})^{n+\frac{1}{2}}_{i^1,j} - (\sigma^h_{xx})^{n+\frac{1}{2}}_{i,j} + (\sigma^b_{xx})^{n+\frac{1}{2}}_{i^1,j^1} - (\sigma^b_{xx})^{n+\frac{1}{2}}_{i,j^1}\right) \ , \\
&\frac{(v_x^y)^{n+1}_{i\frac{1}{2},j\frac{1}{2}} - (v_x^y)^n_{i\frac{1}{2},j\frac{1}{2}}}{\Delta t} + d^y_{i\frac{1}{2}}\frac{(v_x^y)^{n+1}_{i\frac{1}{2},j\frac{1}{2}} + (v_x^y)^n_{i\frac{1}{2},j\frac{1}{2}}}{2} \\
&= \frac{1}{2\varrho h}\left((\sigma_{xy})^{n+\frac{1}{2}}_{i,j^1} - (\sigma_{xy})^{n+\frac{1}{2}}_{i,j} + (\sigma_{xy})^{n+\frac{1}{2}}_{i^1,j^1} - (\sigma_{xy})^{n+\frac{1}{2}}_{i^1,j}\right) \ ,
\end{aligned}
$$

$$
\begin{aligned}
&(v_y)^n_{i\frac{1}{2},j\frac{1}{2}} = (v_y^x)^n_{i\frac{1}{2},j\frac{1}{2}} + (v_y^y)^n_{i\frac{1}{2},j\frac{1}{2}} \ , \\
&\frac{(v_y^x)^{n+1}_{i\frac{1}{2},j\frac{1}{2}} - (v_y^x)^n_{i\frac{1}{2},j\frac{1}{2}}}{\Delta t} + d^x_{i\frac{1}{2}}\frac{(v_y^x)^{n+1}_{i\frac{1}{2},j\frac{1}{2}} + (v_y^x)^n_{i\frac{1}{2},j\frac{1}{2}}}{2} \\
&= \frac{1}{2\varrho h}\left((\sigma_{xy})^{n+\frac{1}{2}}_{i^1,j} - (\sigma_{xy})^{n+\frac{1}{2}}_{i,j} + (\sigma_{xy})^{n+\frac{1}{2}}_{i^1,j^1} - (\sigma_{xy})^{n+\frac{1}{2}}_{i,j^1}\right) \ , \\
&\frac{(v_y^y)^{n+1}_{i\frac{1}{2},j\frac{1}{2}} - (v_y^y)^n_{i\frac{1}{2},j\frac{1}{2}}}{\Delta t} + d^y_{i\frac{1}{2}}\frac{(v_y^y)^{n+1}_{i\frac{1}{2},j\frac{1}{2}} + (v_y^y)^n_{i\frac{1}{2},j\frac{1}{2}}}{2} \\
&= \frac{1}{2\varrho h}\left((\sigma^d_{yy})^{n+\frac{1}{2}}_{i,j^1} - (\sigma^d_{yy})^{n+\frac{1}{2}}_{i,j} + (\sigma^g_{yy})^{n+\frac{1}{2}}_{i^1,j^1} - (\sigma^g_{yy})^{n+\frac{1}{2}}_{i^1,j}\right) \ ,
\end{aligned}
$$

and

$$
\begin{aligned}
&\Sigma^{n+\frac{1}{2}}_{i,j} = (\Sigma^x)^{n+\frac{1}{2}}_{i,j} + (\Sigma^y)^{n+\frac{1}{2}}_{i,j} \ , \\
&\frac{(\Sigma^x)^{n+\frac{1}{2}}_{i,j} - (\Sigma^x)^{n-\frac{1}{2}}_{i,j}}{\Delta t} + d^x_i\frac{(\Sigma^x)^{n+\frac{1}{2}}_{i,j} + (\Sigma^x)^{n-\frac{1}{2}}_{i,j}}{2} = A_h^{-1}B_h^x, \\
&\frac{(\Sigma^y)^{n+\frac{1}{2}}_{i,j} - (\Sigma^y)^{n-\frac{1}{2}}_{i,j}}{\Delta t} + d^y_i\frac{(\Sigma^y)^{n+\frac{1}{2}}_{i,j} + (\Sigma^y)^{n-\frac{1}{2}}_{i,j}}{2} = A_h^{-1}B_h^y.
\end{aligned}
$$

The properties of this model are studied in terms of a numerical dispersion analysis presented in Appendix A. This analysis permits us to compute the reflection coefficients in the case of a homogeneous, isotropic elastic solid. In this case we have found that the reflection coefficients are roughly proportional to h^2. That shows the second order accuracy of the discrete PML model, which is thus no longer perfectly matched. This means in particular that the damping factor can not be chosen to be too large with respect to the inverse of the discretization step. Of course, it must be large enough to allow the damping of the wave inside the layer. So there is a trade off to be found (see the end of the appendix for more details).

Remark 3 *The theoretical results presented in the previous sections are based on a plane wave analysis and thus they can be applied only to wave propagation problems in homogeneous media. However, as we will see in the next sections the discrete PML model can be also used to compute numerically the solution of the elastodynamic problem in heterogeneous anisotropic elastic media although we have no theoretical justification for this extension.*

NUMERICAL RESULTS

In the following examples, we simulate elastic wave propagation in a 2-D unbounded medium. We will present several results including the case of heterogeneous, anisotropic elastic media. In order to show the generality of the method we give some numerical results for both schemes : the Virieux finite-difference scheme and the finite-element scheme. A more complete analysis is presented for the finite-element scheme, namely the discrete reflection coefficients are computed as a function of the incident angle. Let us first set some notation and give the characteristics of the numerical examples that will follow. We consider an unbounded domain Ω in 2D, occupied by an elastic material and we suppose that the initial condition (or the source) is supported in a part of Ω. The material will be characterized by its wave velocities V_p (pressure) and V_s (shear) in the isotropic case and by its elasticity matrix C in the anisotropic case. In order to solve numerically the elastodynamic problem in Ω we define a bounded domain D of a simple geometry (here it will be a square), containing the support of the initial data, with absorbing layers (PML) on all four boundaries. For the discretization of the problem we take a regular grid on D composed of $N \times N$ square elements of edge $h = 1/N$. The time step is then computed following the CFL condition for each scheme, more precisely we take : $\Delta t = 0.9h/(\sqrt{2}V_p)$ for the Virieux scheme, and $\Delta t = h/V_p$ for the finite-element scheme.

For our numerical experiments an explosive source located at point $S = (x^s, y^s)$ is used, that is

$$f(x,t) = F(t)\vec{g}(r).$$

The function $F(t)$ is defined by

$$F(t) = \begin{cases} -2\pi^2 f_0^2(t-t_0)e^{-\pi^2 f_0^2 (t-t_0)^2} & \text{if } t \le 2t_0 \\ 0 & \text{if } t > 2t_0 \end{cases}, \tag{18}$$

where $t_0 = 1/f_0$, $f_0 = Vs/(hN_L)$ is the central frequency, and N_L is the number of points per S wave-length. The function $\vec{g}(r)$ is a radial function given by

$$\vec{g}(r) = \left(1 - \frac{r^2}{a^2}\right)^3 1_{B_a} \left(\frac{x-x^s}{r}, \frac{y-y^s}{r}\right), \quad r = \sqrt{(x-x^s)^2 + (y-y^s)^2},\ a = 5h, \tag{19}$$

where 1_{B_a} is one on B_a, the disk of center S and radius a, and zero elsewhere. In the absorbing layers we use the following model for the damping parameter $d(x)$,

$$d(x) = d_0 \left(\frac{x}{\delta}\right)^2, \tag{20}$$

where δ is the width of the layer and d_0 is a function of the theoretical reflection coefficient ($R = R^\delta_{pp}$) (see relation (15) for $\theta = 0$)

$$d_0 = \log\left(\frac{1}{R}\right)\frac{3V_p}{2\delta}. \tag{21}$$

We first present some results in a homogeneous isotropic medium.

Homogeneous, isotropic elastic medium-Virieux scheme

We consider here an elastic medium with $V_p = 2000\text{m/s}$, $V_s = 1400\text{m/s}$. The characteristics of the discretization are

$$N = 200,\ h = 0.15\text{m},\ S = (7.5\text{m}, 7.5\text{m}),$$
$$N_L = 20,\ \delta = 10h \text{ and } R = 0.001.$$

We present some snapshots of the solution in Figure 4.

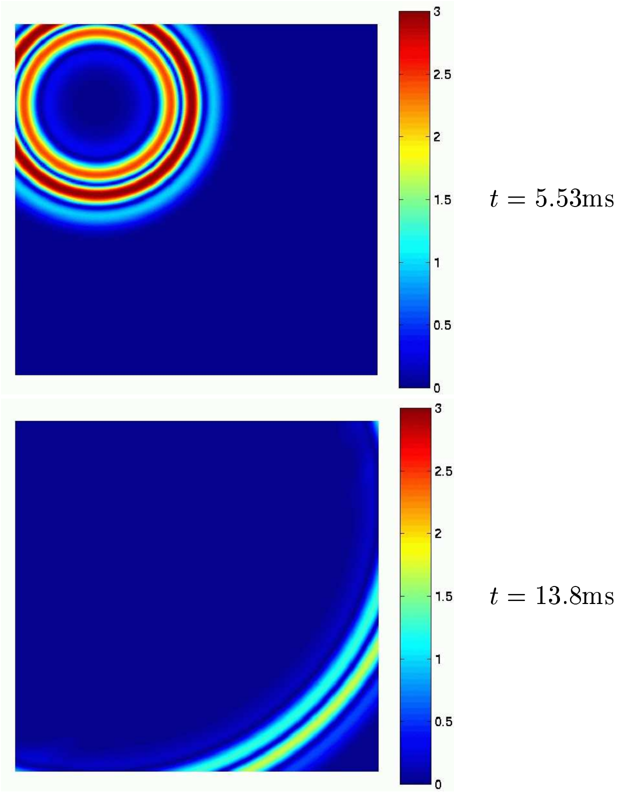

FIG. 4. Snapshots of 2-D elastic finite-difference simulations (Virieux scheme), in a homogeneous medium, using a PML layer with width $10h$. The snapshots are the norm of the velocity $\|v\| = \sqrt{v_1^2 + v_2^2}$

The snapshots presented in Figure 4 show no reflection when the results are presented on the normal scale. Indeed, for the PML model used in this example the reflection coefficient is about 0.1% as it can be seen by magnifying the results by a factor of 100 (see Figure 5). In Figure 5 we also present the results obtained using the 1st order absorbing boundary condition introduced by Reynolds (1978). The reflection coefficient for this ABC is about 10% : the 1st order ABC is not accurate enough for waves traveling obliquely to the boundary.

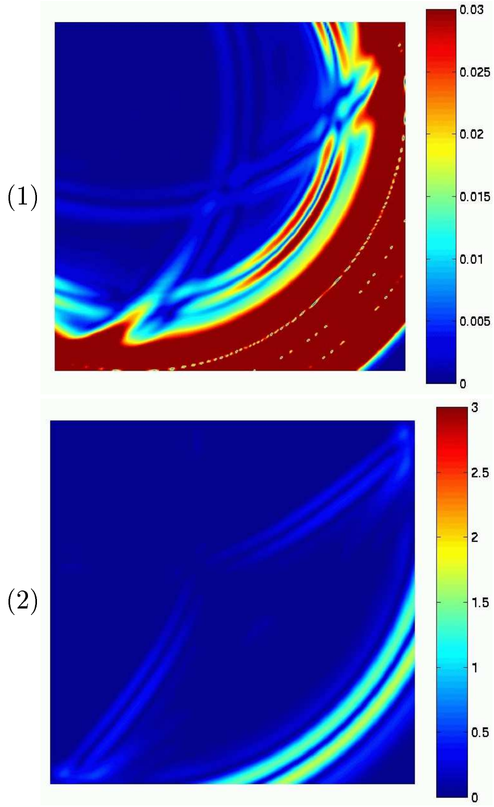

FIG. 5. The the norm of the velocity at $t = 13.8$ms : In (1) we present the results obtained with the PML model ($\delta = 10h$) magnified by a factor of 100 and in (2) we present the results obtained with a 1st order ABC on the normal scale.

Heterogeneous, isotropic elastic medium-Virieux scheme

We consider a heterogeneous elastic medium, the interface is parallel to the x axis and located in the middle of the frame (see Figure 6). The wave velocities in the two media are $V_p^1 = 2000$m/s, $V_s^1 = 1400$m/s (the upper medium), $V_p^2 = 1000$m/s, $V_s^2 = 700$m/s (the lower medium). All the other parameters are the same as in section A where $V_s = (V_s^1 + V_s^2)/2$ has been used for the computation of f_0 (equation 18) and $V_p = V_p^1$ to compute Δt. The source is now located in the lower medium near the interface (at point$(15\text{m}, 16.2\text{m})$). We present some snapshots of the solution in Figure 6.

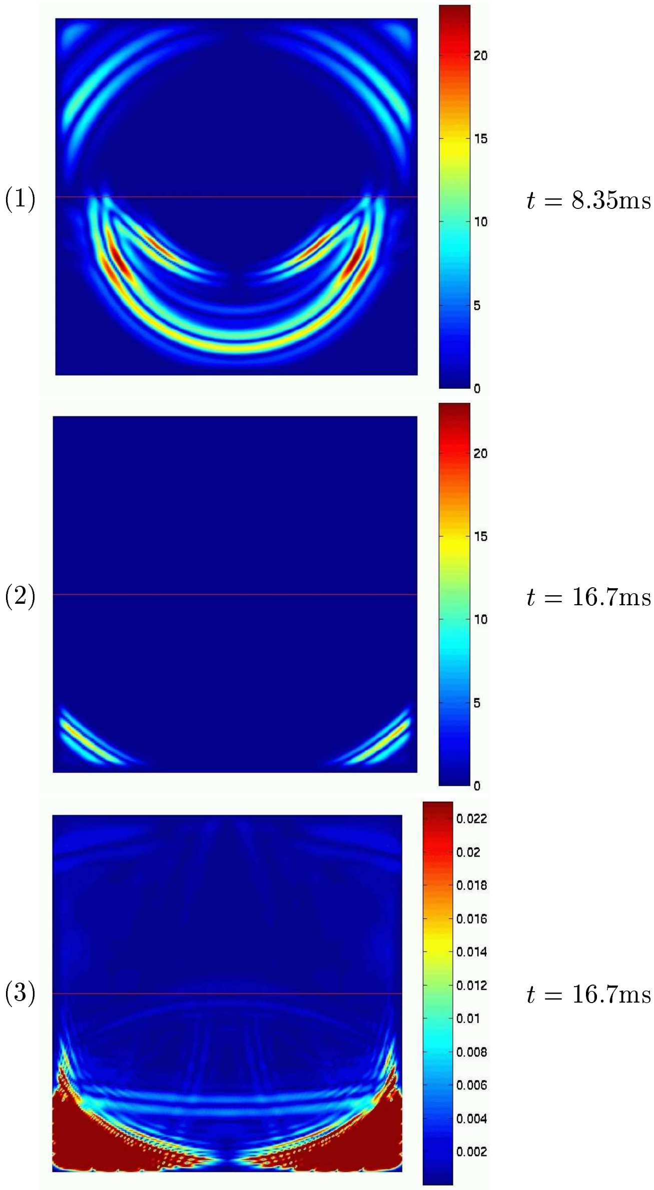

FIG. 6. Snapshots of 2-D elastic finite-differences simulations (Virieux scheme), in a heterogeneous medium, using a PML layer with length $10h$. We present the norm of the velocity $\|v\| = \sqrt{v_1^2 + v_2^2}$, in the normal scale (1) and (2). To see some reflections, (3) is magnified by a factor of 1000.

The reflection coefficient for this example is about 0.1% as we can see in Figure 6.

Heterogeneous, isotropic elastic medium. Finite-element scheme

The heterogeneous elastic medium considered here is characterized by the velocity model presented in Figure 7, we have $\dfrac{\max V_p}{\min V_p} = 2.1$ and $V_p = 1.6V_s$. For the discretization V_p and V_s are piecewise constants (one value per element).

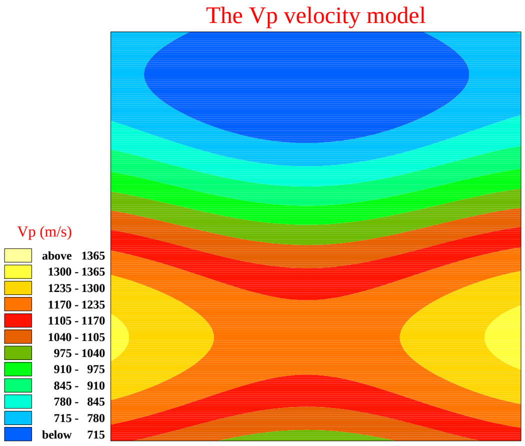

FIG. 7. The velocity model for the heterogeneous medium, $\dfrac{\max V_p}{\min V_p} = 2.1$ and $V_p = 1.6 V_s$.

The size of the grid is 200×200, $h = 0.15$m, $N_L = 10$ and the source is located at point $(15\text{m}, 3\text{m})$. We present, in Figure 8, the norm of the velocity magnified by a factor of 20 for three experiments corresponding to different absorbing layers. More precisely relations (20) and (21) are used with $\delta = 5h - R = 0.01$, $\delta = 10h - R = 0.001$ and $\delta = 20h - R = 0.0001$. Let us recall that these values for R correspond to the theoretical (R_{pp}) reflection coefficients. The reflection coefficients obtained numerically are close to the theoretical ones. This is no longer true if the number of meshes inside the layer is too small : the smaller R the larger layer width required. This phenomenon is due to the numerical dispersion (Collino and Monk, 1998).

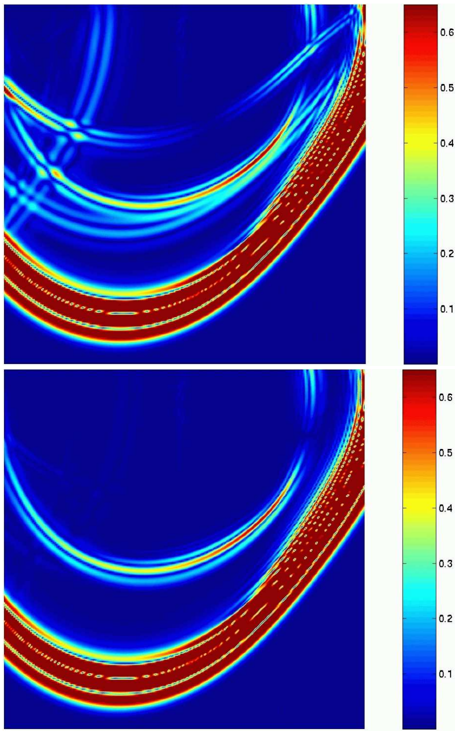

$5h$

$10h$

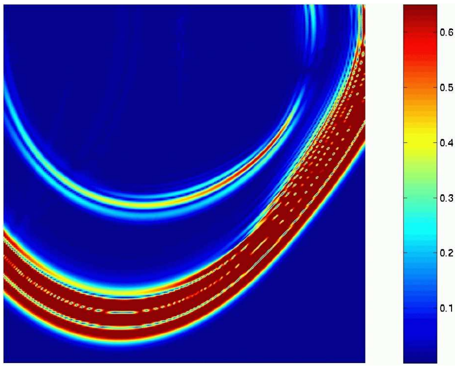

$20h$

FIG. 8. Snapshots of 2-D elastic finite-elements simulations, in a heterogeneous medium, using the PML absorbing layer model with $\delta = 5h$, $\delta = 10h$ and $\delta = 20h$. The snapshots are the norm of the velocity at $t = 14.2$ms magnified by a factor of 20.

Homogeneous, anisotropic elastic medium. Finite-element scheme

In this example we consider an anisotropic elastic solid, the apatite. We want to point out that in the case of anisotropic elastic materials only lower order absorbing boundary conditions are known and they are quite difficult to implement (Bécache, 1991). On the contrary the generalization of the PML model to the anisotropic case is straightforward and there are no supplementary difficulties for the implementation. Moreover the results are very satisfactory as we can see in the following Figures.

The characteristics of the problem are : $N = 200$, $h = 0.15$m, $N_L = 10$ and the source is located at the center of the frame $S = (15\text{m}, 15\text{m})$. We present in Figure 9 three experiments, corresponding to : $\delta = 5h - R = 0.01$, $\delta = 10h - R = 0.001$ and $\delta = 20h - R = 0.0001$.

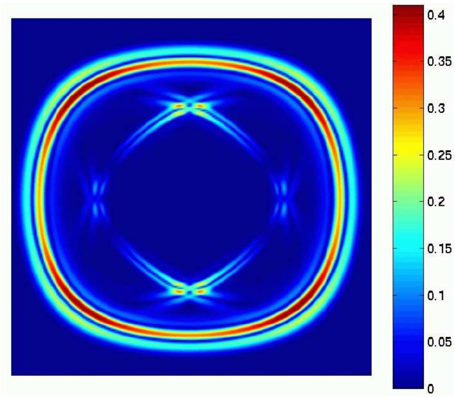

$t = 6.6$ms

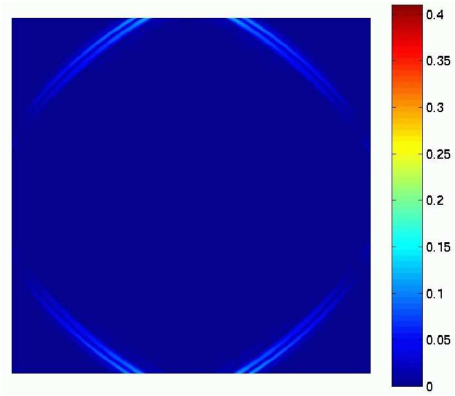

$t = 13.2$ms

FIG. 9. Snapshots of 2-D elastic finite-elements simulations, in an homogeneous anisotropic medium, using the PML absorbing layer model with $\delta = 5h$. The snapshots are the norm of the velocity $\|v\| = \sqrt{v_1^2 + v_2^2}$

We can see in Figure 9 that there is no reflection when the results are presented on the normal scale as it was already the case for an homogeneous medium. However, we can see some reflection by magnifying these results as shown in Figure 10.

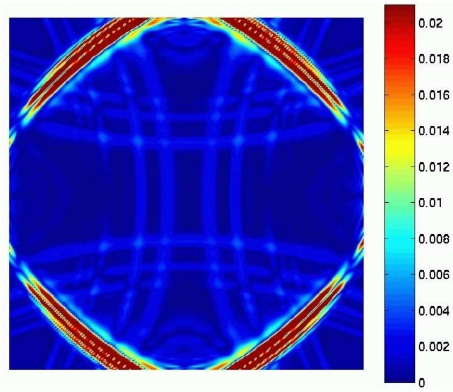

$5h$

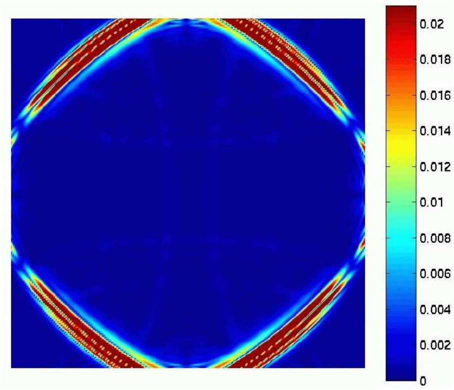

$10h$

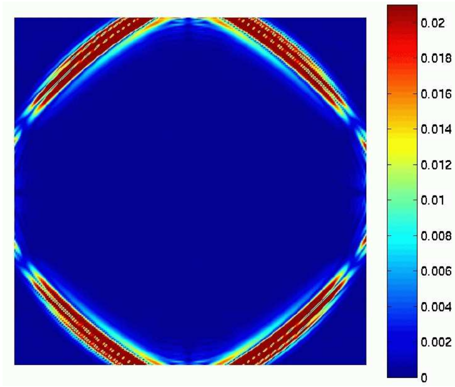

$20h$

FIG. 10. Snapshots of 2-D elastic finite-elements simulations, in an homogeneous anisotropic medium, using the PML absorbing layer model with $\delta = 5h$, $\delta = 10h$ and $\delta = 20h$. The snapshots are the norm of the velocity at $t = 13.2$ms magnified by a factor of 20.

The reflection coefficients obtained numerically are close to the theoretical ones.

Reflection Coefficients

In this section reflection coefficients computed using numerical simulations are shown. We consider a homogeneous isotropic elastic solid ($V_p = 5.710$m/s, $V_s = 2.93$m/s) and we use the finite-element scheme for the space discretization. To compute the reflection coefficients we first consider the solution of the elastodynamic problem at points M_i located near the upper boundary of domain D_1 (D_1 is a rectangular domain of size 200m$\times$100m and a PML layer model is used on all boundaries of the domain). We denote by $(V_1)_i$ the velocity vector at point M_i. Then to obtain a reference solution at points M_i we move the upper boundary of the domain 50m above. That is, we solve the elastodynamic problem in the domain D_2 (a rectangle of size 200m $\times$ 150m). We also use the PML layer model on all boundaries of the domain and we denote by $(V_2)_i$ the velocity vector at point M_i. The geometry of the problem with the two computational domains is shown in Figure 11.

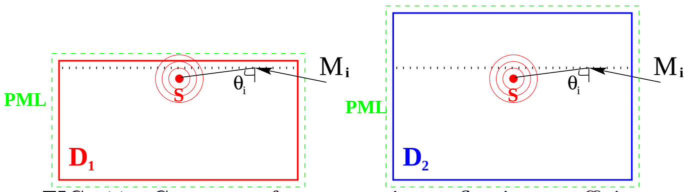

FIG. 11. Geometry for computing reflection coefficients. Two computational domains are defined : D_1 200m $\times$ 100m and D_2 200m $\times$ 150m.

In the case of a pure P-wave source we define the reflection coefficients by,

$$
\begin{aligned}
(R_{pp})(\theta_i) &= \frac{\mathrm{div}(U_2)_i - \mathrm{div}(U_1)_i}{\mathrm{div}(U_2)_i} \ , \\
(R_{ps})(\theta_i) &= \frac{\mathrm{curl}(U_2)_i - \mathrm{curl}(U_1)_i}{\mathrm{curl}(U_2)_i} \ .
\end{aligned}
\tag{22}
$$

In the same way we define

$$
\begin{aligned}
(R_{ss})(\theta_i) &= \frac{\mathrm{curl}(U_2) - \mathrm{curl}(U_1)}{\mathrm{curl}(U_2)} \ , \\
(R_{sp})(\theta_i) &= \frac{\mathrm{div}(U_2) - \mathrm{div}(U_1)}{\mathrm{div}(U_2)} \ ,
\end{aligned}
$$

in the case of a pure S wave source. For our examples we use the P-wave source function given by (18,19) with $N_L = 16$. For this source function the curl of the velocity is smaller than the divergence by a factor 10^{-10}: the reflection coefficient R_{ps} is neglected.

Remark 4 *Relation (22) is used to compute two reflection coefficients at each time step. The results presented in Figure 12 correspond to their mean value over* $[0, T]$*, for* $T = 25sec$.

The grid size is 400×200 for D_1, 400×300 for D_2 and $h = 0.5$m for both domains. The source is located at point $(200, 80)$ of the grid. In the PML layers,

$$
d(x) = d_0 \left(\frac{x}{\delta}\right)^4 \ , \tag{23}
$$

where δ is the length of the layer and d_0 is given by

$$
d_0 = \log\left(\frac{1}{R}\right)\frac{4V_p}{2\delta} \ .
$$

We present three experiments with $\delta = 5h - R = 10^{-4}$, $\delta = 10h - R = 10^{-6}$ and $\delta = 20h - R = 10^{-8}$. To examine the performance of the PML model, comparisons with the 1st, 2nd and 3rd order Higdon's absorbing boundary conditions are performed.

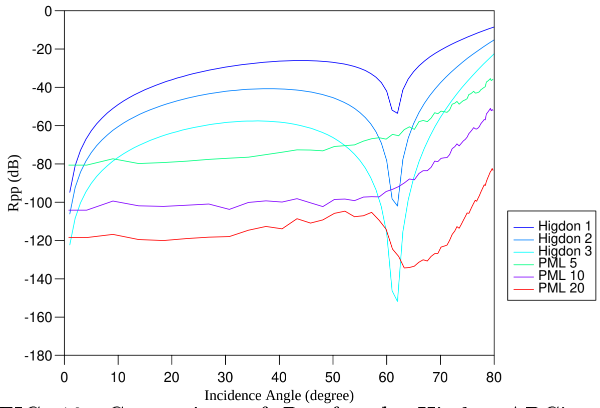

FIG. 12. Comparison of R_{pp} for the Higdon ABC's and PML.

Remark 5 *The reflection coefficients for the absorbing boundary conditions proposed by Higdon are the theoretical ones. We obtain them by applying an operator of the form*

$$
\prod_{i=1}^{m}\left(\beta_i \frac{\partial}{\partial t} + V_p \frac{\partial}{\partial n}\right) \ ,
$$

with $m = 1$; $\beta_1 = 1$, *or* $m = 2$; $\beta_1 = 1$, $\beta_2 = V_p/V_s(= 1.95)$, *or* $m = 3$; $\beta_1 = 1$, $\beta_2 = 1.5$, $\beta_3 = V_p/V_s(= 1.95)$.

As we can see in Figure 18 for almost all angles of incidence the PML absorbing layer model gives better results then the absorbing boundary conditions of first and second order and this even for the $5h$ length absorbing layer. Compared to the third order absorbing condition the PML layers of $10h$ and $20h$ are substantially better except near the $60°$ degree angle. We want to point out that in this example we compare the reflection coefficients provided by the continuous Higdon model to the one given by the discrete PML model. It is known that the Higdon reflection coefficients increase when discretization is used.

The numerical results presented in the sections above show the generality of the PML model: these models can be easily implemented in different numerical schemes. They give satisfactory results even in the case of anisotropic heterogeneous elastic media. The reflection coefficients are close to the theoretical ones for all the presented experiments. They are about 1% for a $5h$ PML layer width, 0.1% for a $10h$ PML layer width and 0.01% for a $20h$ PML layer width in all experiments. In practice one should choose the length of the layer as a function of the scale of the problem and the requested reflection coefficient. In the numerical examples that we have presented the scale of the problems was about 15 wavelengths of P-wave (λ_p) in each direction, in this case a PML layer with $\delta = 5h$ (that is about 0.5 λ_p) is sufficient and gives better results than the second order absorbing condition. However, for larger scale computations the numerical dispersion will be more important and thus a PML layer with $\delta = 5h$ would probably not give the expected results. Thus for large scale problems one should consider a PML layer with $\delta \geq 10h$. We want to point out, that even in this case the additional cost remains modest, given that the layer only represents a small portion of the total grid. Let us finally remark that the PML model can be easily extended to the case of Rayleigh waves. (Experimental results not shown in this paper have demonstrated a good absorption of Rayleigh waves).

CONCLUSIONS

We have presented in this paper a generalization of the PML absorbing layer model for the elastodynamic problem in the case of heterogeneous, anisotropic media. The implementation of this model was presented in the 2D case but it can be straightforwardly extended to the 3D case. The superiority of this model compared with the absorbing boundary conditions proposed by Higdon was shown by numerical results in the case of an isotropic homogeneous medium. Moreover we have shown by several numerical examples the efficiency of this model even in the case of heterogeneous, anisotropic media. To conclude, let us point out the ease of the implementation of this model in the case of an anisotropic elastic medium in comparison with the complexity of the respective absorbing boundary conditions.

REFERENCES

Achenbach, J. D., 1984, Wave propagation in elastic solids:, volume I and II Elsevier Science Publ. B.V.

Auld, B. A., 1973, Acoustic fields and elastic waves in solids: John Wiley & Sons, Inc.

Bécache, E., Joly, P., and Tsogka, C., 1997, Eléments finis mixtes et condensation de masse en élastodynamique linéaire. (i) construction: C. R. Acad. Sci. Paris Sér. I Math., **325**, 545–550.

Bécache, E., Joly, P., and Tsogka, C., 1998, Fictitious domain method applied to the scattering by a crack of transient elastic waves in anisotropic media : a new family of mixed finite elements leading to explicit schemes: Mathematical and numerical aspects of wave propagation, SIAM, 322–326.

Bécache, E., 1991, Résolution par une méthode d'équations intégrales d'un problème de diffraction d'ondes élastiques transitoires par une fissure.: Ph.D. thesis, Univ. of Paris 6.

Bérenger, J., 1994, A perfectly matched layer for the absorption of electromagnetic waves: J. Comput. Phys., **114**, 185–200.

Bérenger, J., 1996, Three-dimensional perfectly matched layer for the absorption of electromagnetic waves: J. Comput. Phys., **127**, 363–379.

Bérenger, J., 1997, Improved PML for the FDTD Solution of Wave-Structure Interaction Problems : IEEE Trans. Antennas and Propagation, **45**, 466–473.

Chalindar, B., 1987, Conditions aux limites artificielles pour les équations de l'élastodynamique: Ph.D. thesis, Univ. Saint Etienne.

Collino, F., and Monk, P., 1998, Optimizing the perfectly matched layers: Comput. Methods Appl. Mech. Engrg., **164**, no. 1-2.

Collino, F., 1996, Perfectly matched absorbing layers for the paraxial equations: J. Comput. Phys., **131**, 164–180.

Engquist, B., and Majda, A., 1977, Absorbing boundary conditions for the numerical simulation of waves: Math. Comp., **31**, 629–651.

Hagstrom, T., 1997, On high-order radiation boundary condition, *in* Engquist, B., and Kriegsmann, G. A., Eds., Computational Wave Propagation: Springer-Verlag New York, Inc., **86**, 1–21.

Hastings, F., Schneider, J., and Broschat, S. L., 1996, Application of the perfectly matched layer (PML) absorbing boundary condition to elastic wave propagation : J. Acoust. Soc. Am., **100**, 3061– 3069.

Higdon, R., 1990, Radiation boundary conditions for elastic wave propagation: SIAM J. Numer. Anal., **27**, 831–870.

Higdon, R., 1991, Absorbing boundary conditions for elastic waves : Geophysics, **56**, 231–241.

Higdon, R., 1992, Absorbing boundary conditions for acoustic and elastic waves in stratified media: J. Comput. Phys., **101**, 386–418.

Israeli, M., and Orszag, S., 1981, Approximation of radiation boundary conditions: J. Comput. Phys., **41**, 115–135.

Peng, C., and Toksoz, M., 1995, An optimal absorbing boundary condition for elastic wave modeling : Geophysics, **60**, 296–301.

Rappaport, C., 1995, Perfectly Matched Absorbing Conditions Based on Anisotropic Lossy Mapping of Space: IEEE Microwave and Guided Wave Letters., **5**, no. 3, 90–92.

Reynolds, A., 1978, Boundary conditions for the numerical solution of wave propagation problems: Geophysics, **43**, 1099–1110.

Simone, A., and Hestholm, S., 1998, Instability in applying absorbing boundary conditions to high-order seismic modeling algorithms : Geophysics., **63**, 1017–1023.

Sochacki, J., Kubichek, R., George, J., Fletcher, W., and Smithson, S., 1987, Absorbing boundary conditions and surface waves : Geophysics, **52**, 60–71.

Teixeira, F. L., and Chew, W. C., 1998, Analytical derivation of a conformal perfectly matched absorber for electromagnetic waves: Micro. Opt. Tech. Lett., **17**, 231–236.

Turkel, E., and Yefet, A., 1998, Absorbing pml boundary layers for wave-like equations. absorbing boundary conditions.: Appl. Numer. Math., **27**, no. 4, 553–557.

Virieux, J., 1986, P-sv wave propagation in heterogeneous media :velocity-stress finite difference method: Geophysics, **51**, 889–901.

Zhao, L., and Cangellaris, A., 1996, A general approach to for developping unsplit-field time-domain implementations of perfectly matched layers for FDTD grid truncation: IEEE Trans. Microwave Theory Tech., **44**, 2555–2563.

APPENDIX A–DISPERSION ANALYSIS

In this section we will study the properties of the discrete PML model for elastodynamics in terms of a numerical dispersion analysis, that is a plane wave analysis. We present this analysis only for the finite-element scheme. We consider the case of an homogeneous isotropic elastic medium characterized by the Lam coefficients λ, μ and the density ϱ. We use an infinite PML layer in the x-direction. We look for plane wave solutions of the form

$$\begin{aligned}
&(V^l)^{n+\frac12}_{i^{\frac12},j^{\frac12}} = (\widehat{V}^l)_{i^{\frac12}} \exp[-ik_y(j^{\frac12})h + i\omega(n+\frac12)\Delta t],\\
&(\Sigma^l)^n_{i,j} = (\widehat{\Sigma}^l)_i \exp[-ik_y jh + i\omega n\Delta t],\\
&V^l = [v^l_x, v^l_y]^T,\ \Sigma^l = [\sigma^{h,l}_{xx}, \sigma^{b,l}_{xx}, \sigma^{d,l}_{yy}, \sigma^{g,l}_{yy}, \sigma, l_{xy}]^T,
\end{aligned}$$

for $l = \perp,\ \parallel$ and we set

$$(\widehat{V})_{i^{\frac12}} = (\widehat{V}^{\parallel})_{i^{\frac12}} + (\widehat{V}^{\perp})_{i^{\frac12}}\ ;\ (\widehat{\Sigma})_i = (\widehat{\Sigma}^{\parallel})_i + (\widehat{\Sigma}^{\perp})_i$$

Plugging these expressions into the discrete scheme and eliminating the unknowns associated to σ, lead to

$$\begin{aligned}
\frac{A_t^2}{\Delta t^2}(\hat v_x)_{i^{\frac12}} &= \frac{\mu}{\varrho}A_y^2\frac{(\hat v_x)_{i^{\frac32}} + 2(\hat v_x)_{i^{\frac12}} + (\hat v_x)_{i^{-\frac12}}}{4h^2}\\
&+\frac{a + c\cos(k_y h)}{\varrho D_{i^{\frac12}}}\left(\frac{(\hat v_x)_{i^{\frac32}} - (\hat v_x)_{i^{\frac12}}}{h^2 D_{i^1}} - \frac{(\hat v_x)_{i^{\frac12}} - (\hat v_x)_{i^{-\frac12}}}{h^2 D_i}\right)\\
&-A_y\frac{\mu}{\varrho}\cos\left(\frac{k_y h}{2}\right)\left(\frac{(\hat v_y)_{i^{\frac32}} - (\hat v_y)_{i^{\frac12}}}{2h^2 D_{i^1}} + \frac{(\hat v_y)_{i^{\frac12}} - (\hat v_y)_{i^{-\frac12}}}{2h^2 D_i}\right.\\
&\left.+\frac{(\hat v_y)_{i^{\frac32}} - (\hat v_y)_{i^{-\frac12}}}{h^2 D_{i^{\frac12}}}\right)\ ,
\end{aligned}\tag{A-1}$$

$$\begin{aligned}
\frac{A_t^2}{\Delta t^2}(\hat v_y)_{i^{\frac12}} &= \frac{1}{\varrho}A_y^2\frac{c(\hat v_y)_{i^{\frac32}} + 2a(\hat v_y)_{i^{\frac12}} + c(\hat v_y)_{i^{-\frac12}}}{2h^2}\\
&+\frac{\mu}{\varrho}\cos^2\left(\frac{k_y h}{2}\right)\left(\frac{(\hat v_y)_{i^{\frac32}} - (\hat v_y)_{i^{\frac12}}}{h^2 D_{i^1} D_{i^{\frac12}}} - \frac{(\hat v_y)_{i^{\frac12}} - (\hat v_y)_{i^{-\frac12}}}{h^2 D_i D_{i^{\frac12}}}\right)\\
&-A_y\frac{b}{\varrho}\cos\left(\frac{k_y h}{2}\right)\left(\frac{(\hat v_x)_{i^{\frac32}} - (\hat v_x)_{i^{\frac12}}}{h^2 D_{i^1}} + \frac{(\hat v_x)_{i^{\frac12}} - (\hat v_x)_{i^{-\frac12}}}{h^2 D_i}\right.\\
&\left.+\frac{(\hat v_x)_{i^{\frac32}} - (\hat v_x)_{i^{-\frac12}}}{2h^2 D_{i^{\frac12}}}\right)\ ,
\end{aligned}\tag{A-2}$$

where $a,\ b,\ c$ are given by (17) and A_t, A_y, C_l and D_l are defined by

$$\begin{aligned}
&A_t = 2i\sin\left(\frac{\omega\Delta t}{2}\right),\ A_y = 2i\sin\left(\frac{k_y h}{2}\right)\ ,\\
&C_l = 2i\sin\left(\frac{\omega\Delta t}{2}\right) + d_l\ \Delta t\cos\left(\frac{\omega\Delta t}{2}\right),\ l = i, i^{\frac12}\ ,\\
&D_l = \frac{C_l}{A_t}, l = i,\ i^{\frac12}\ .
\end{aligned}$$

Let us consider now the case of a medium with a unique infinite layer for which

$$d_i = \begin{cases} 0 & \text{if } i \le 0 \\ d_\infty & \text{if } i > 0 \end{cases}\ ,\ d_{i^{\frac12}} = \begin{cases} 0 & \text{if } i < 0 \\ d_\infty & \text{if } i > 0 \end{cases}\ ,$$

$d_{\frac12}$ remaining undetermined yet, and let us look for particular solution of the form

P wave

$$\begin{aligned}
(\widehat{V})_{i^{\frac12}} &= \vec{d}_p e^{-ik_x(i^{\frac12})h} + R_{pp}\vec{d}^r_p e^{ik_x(i^{\frac12})h}\\
&+R_{ps}\vec{d}^r_s e^{ik_x(i^{\frac12})h} \qquad \text{for } i^{\frac12} \le 0\ ,\\
(\widehat{V})_{i^{\frac12}} &= T_{pp}\widetilde{d}_p e^{-i\widetilde{k}_x(i^{\frac12})h} + T_{ps}\widetilde{d}_s e^{-i\widetilde{k}_x(i^{\frac12})h} \quad \text{for } i^{\frac12} \ge 0\ .
\end{aligned}$$

S wave

$$\begin{aligned}
(\widehat{V})_{i^{\frac12}} &= \vec{d}_s e^{-ik_x(i^{\frac12})h} + R_{ss}\vec{d}^r_s e^{ik_x(i^{\frac12})h}\\
&+R_{sp}\vec{d}^r_p e^{ik_x(i^{\frac12})h} \qquad \text{for } i^{\frac12} \le 0\ ,\\
(\widehat{V})_{i^{\frac12}} &= T_{ss}\widetilde{d}_s e^{-i\widetilde{k}_x(i^{\frac12})h} + T_{sp}\widetilde{d}_p e^{-i\widetilde{k}_x(i^{\frac12})h} \quad \text{for } i^{\frac12} \ge 0\ .
\end{aligned}$$

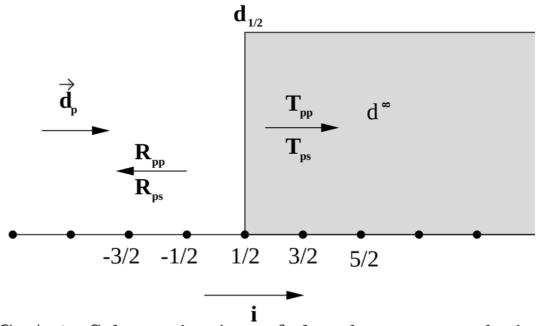

FIG. A-1. Schematic view of the plane wave solution in a single layer discrete model

The equations (A-1) and (A-2) are satisfied for $i^{\frac12} \neq 0$ if k_x and $\widetilde{k}_x$ are solutions of the two relations of dispersion (A-3) (free medium) and (A-4) (lossy medium).

$$\frac{X_t^2}{\Delta t^2}\begin{bmatrix}\hat v_x\\ \hat v_y\end{bmatrix} = \frac{1}{h^2}\begin{bmatrix}\hat K_{11} & \hat K_{12}\\ \hat K_{12} & \hat K_{22}\end{bmatrix}\begin{bmatrix}\hat v_x\\ \hat v_y\end{bmatrix}\ , \tag{A-3}$$

$$\frac{X_t^2}{\Delta t^2}\begin{bmatrix}\hat v_x\\ \hat v_y\end{bmatrix} = \frac{1}{h^2}\begin{bmatrix}\widetilde{K}_{11} & \widetilde{K}_{12}\\ \widetilde{K}_{12} & \widetilde{K}_{22}\end{bmatrix}\begin{bmatrix}\hat v_x\\ \hat v_y\end{bmatrix}\ , \tag{A-4}$$

with

$$\hat{K}_{11} = V_p^2 X_x(1-4\alpha X_y) + V_s^2 X_y(1-\beta X_x) \ ,$$
$$\hat{K}_{22} = V_p^2 X_y(1-4\alpha X_x) + V_s^2 X_x(1-\beta X_y) \ ,$$
$$\hat{K}_{12} = (V_p^2 - V_s^2)\sqrt{X_x X_y (1-X_x)(1-X_y)} \ ,$$

$$X_t = \sin^2\left(\frac{\omega\Delta t}{2}\right), \ X_x = \sin^2\left(\frac{k_x h}{2}\right) \ ,$$
$$X_y = \sin^2\left(\frac{k_y h}{2}\right), \ \alpha = \frac{(V_p^2 - 2V_s^2)^2}{4V_p^4}, \ \beta = \frac{1}{4} \ ,$$

and

$$\widetilde{K}_{11} = V_p^2 \frac{\widetilde{X}_x}{\widetilde{D}^2}(1-4\alpha X_y) + V_s^2 X_y(1-\beta\widetilde{X}_x) \ ,$$
$$\widetilde{K}_{22} = V_p^2 X_y(1-4\alpha\widetilde{X}_x) + V_s^2 \frac{\widetilde{X}_x}{\widetilde{D}^2}(1-\beta X_y) \ ,$$
$$\widetilde{K}_{12} = \frac{(V_p^2 - V_s^2)}{\widetilde{D}}\sqrt{\widetilde{X}_x X_y(1-\widetilde{X}_x)(1-X_y)} \ ,$$
$$\widetilde{X}_x = \sin^2\left(\frac{\widetilde{k}_x h}{2}\right), \ \widetilde{D} = \frac{2i\sin\left(\frac{\omega\Delta t}{2}\right) + d_\infty \ \Delta t\cos\left(\frac{\omega\Delta t}{2}\right)}{2i\sin\left(\frac{\omega\Delta t}{2}\right)}.$$

Now, the system of equations (A-3) and (A-4) at $i^{\frac{1}{2}} = 0$ gives the value of the reflection coefficients R_{pp}(resp. R_{ss}) and R_{ps}(resp. R_{sp}). We have used the software MAPLE to compute their Taylor expansions with respect to the discretization step h and we obtained

$$\begin{aligned}
R_{pp} &= \frac{d_\infty - 2d_{\frac{1}{2}}}{4\omega}\left(1 - 2r_1^2(V_p^2+V_s^2)\right)\frac{r_0}{V_p}h + O(h^2) \ ,\\
R_{ps} &= \frac{d_\infty - 2d_{\frac{1}{2}}}{4\omega}\left(3 - 2r_1^2(V_p^2+V_s^2)\right)k_y h + O(h^2) \ ,\\
R_{ss} &= \frac{d_\infty - 2d_{\frac{1}{2}}}{4\omega}\left(1 - 2r_2^2 r_1^2(V_p^2+V_s^2)\right)\frac{r_0}{V_p}h + O(h^2) \ ,\\
R_{sp} &= \frac{d_\infty - 2d_{\frac{1}{2}}}{4\omega}\left(2r_2^2 r_1^2(V_p^2+V_s^2) - 1 - 2r_2^2\right)k_y h + O(h^2) \ ,
\end{aligned} \tag{A-5}$$

with

$$r_0 = \sqrt{\omega^2 - V_p^2 k_y^2}, \ r_1 = \frac{k_y^2}{\omega^2}, \ r_2 = \frac{V_s^2}{V_p^2}, \ r_3 = \frac{1}{r_2} \ .$$

From relations (A-5), we can easily remark that the best choice for $d_{\frac{1}{2}}$ consists in taking

$$d_{\frac{1}{2}} = \frac{d_\infty}{2} \ .$$

In that case, the first order terms in (A-5) disappear and we obtain that the reflection coefficients are roughly proportional to $d_\infty(d_\infty + i\omega)h^2$. Two consequences can be deduced from this result. First the numerical scheme is consistent with the continuous PML model : the spurious reflection for a given value of d_∞ is only due to the dispersion of the numerical scheme. Let us remark that the second order accuracy is recovered in the h^2 dependency of the reflection coefficients. Then, from a more practical point of view, this dispersion analysis implies that we cannot use a value of d_∞ too large for a given discretization step.

In the case of a finite length layer with a given number of nodes, the layer is characterized by

$$\begin{cases} (d_{\frac{1}{2}}, \ d_{\frac{3}{2}}, \ ..., d_{n_l - \frac{1}{2}}), \\ (d_1, \ d_2, \ ..., d_{n_l}), \end{cases}$$

we are then led to find a trade off between choosing the $d_{i+\frac{1}{2}}$'s too small (which would imply a strong reflection due to the Dirichlet boundary condition) or too large (which would imply spurious reflections due to the dispersion). A partial answer to this problem is to use a smooth profile for $d(x)$, ($d_{i+\frac{1}{2}} = d(h(i+\frac{1}{2}))$), as is done in the classical layers models, (Israeli and Orszag, 1981). An alternative is to determine the best coefficients for $d(x)$ by minimizing the numerical reflection coefficients as is done in (Collino and Monk, 1998) for the Helmholtz equation.